Synthesis of Hydroxyapatite/Zinc Oxide Nanoparticles from Fish Scales for the Removal of Hydrogen Sulfide

Dan-Thuy Van-Pham[1], Vien Vinh Phat[1], Nguyen Huu Chiem[2], Tran Thi Bich Quyen[1], Ngo Truong Ngoc Mai[1], Dang Huynh Giao[1], Ta Ngoc Don[3], and Doan Van Hong Thien[1*]

[1]Department of Chemical Engineering, Can Tho University, 3/2 Street, Ninh Kieu District, Can Tho City, Vietnam
[2]Department of Environmental Sciences, Can Tho University, 3/2 Street, Ninh Kieu District, Can Tho City, Vietnam
[3]Ministry of Education and Training, No 35, Dai Co Viet, Hanoi, Vietnam

ARTICLE INFO

Received: 21 Nov 2021
Received in revised: 28 Feb 2022
Accepted: 4 Mar 2022
Published online: 1 Apr 2022
DOI: 10.32526/ennrj/20/202100228

Keywords:
Hydrogen sulfide/ Hydroxyapatite/ Room temperature/ Zinc oxide

*** Corresponding author:**
E-mail: dvhthien@ctu.edu.vn

ABSTRACT

The presence of hydrogen sulfide (H_2S) is an issue for industrial processing, such as gasoline, natural gas, and biogas. In this study, hydroxyapatite (HA) nanoparticles with high purity were successfully extracted from red tilapia fish scales and used as supporting materials for zinc oxide (ZnO) to remove H_2S. Various amounts of ZnO decorated on HA nanoparticles were prepared from a zinc nitrate hexahydrate precursor. Powder X-ray diffraction (XRD) and Fourier transform infrared spectroscopy (FTIR) of the ZnO/HA samples demonstrated the successful synthesis of ZnO/HA with high purity. The scanning electron microscope (SEM) image analysis confirmed the uniform deposition of ZnO on HA nanoparticles which were smaller than 245 nm. The ZnO/HA samples with different ZnO loadings (i.e., 5, 10, and 15 wt%) were used to remove H_2S at room temperature. The specific surface area of HA and ZnO/HA determined by the Brunauer-Emmett-Teller (BET) method was 37.022 (m^2/g) and 111.609 (m^2/g), respectively. The experimental results demonstrated the highest breakthrough sulfur capacity of 26.3 mg S/g with the sorbent ZnO (15 wt%)/HA nanoparticles. This H_2S adsorption capacity was the highest capacity ever achieved for ZnO/HA.Therefore, there are great possibilities for effective removal of H_2S at the ambient conditions using the ZnO (15 wt%)/HA nanoparticles, where HA nanoparticles could be sustainably extracted from the abundant organic source of red tilapia fish scales.

1. INTRODUCTION

Hydrogen sulfide (H_2S) is one of the most difficult issues for energy industries such as natural gas, biogas, liquefied gas, and gasoline since it causes the corrosion of pipes and equipment, and poisons catalysts even at low concentrations (de Falco et al., 2018; Gupta et al., 2021; Han et al., 2020; Liu et al., 2012; Qiu et al., 2021). H_2S is usually treated by biological, physical and chemical methods (Gupta et al., 2021; Qiu et al., 2021; Wang et al., 2021). Among them, the chemical treatment method, particularly chemical adsorption, has the highest removal efficiency (Ali et al., 2020a; Ali et al., 2020b; Ali and Saleh, 2020; de Falco et al., 2018; Gupta et al., 2021; Qiu et al., 2021; Quan et al., 2021; Saleh, 2020; Saleh, 2021b; Singh et al., 2019). Metal oxides are often used as chemical adsorbents for high performance. For example, zinc oxide (ZnO) is a well-known photocatalyst for the degradation of several environmental contaminants due to being a non-toxic and inexpensive material with a high capacity to adsorb H_2S (Buazar et al., 2015). Moreover, it has been known to have a high equilibrium constant for H_2S removal at the ambient temperature ranging from 5.9 mg S/adsorbent to nearly 96.5 mg S/adsorbent (Al-Hammadi et al., 2018; Al-Jamimi and Saleh, 2019; de Falco et al., 2018; Geng et al., 2019; Gupta et al., 2021; Saleh et al., 2019; Saleh et al., 2020).

There are various ways to synthesize ZnO NPs (Buazar et al., 2016a; Buazar et al., 2016b). However, there are some difficulties in using ZnO directly as an adsorbent. The main drawback reported by previous

Citation: Van-Pham D-T, PhatVV, Chiem NH, Quyen TTB, Mai NTN, Giao DH, Don TN, Thien DVH. Synthesis of hydroxyapatite/zinc oxide nanoparticles from fish scales for the removal of hydrogen sulfide. Environ. Nat. Resour. J. 2022;20(3):323-329. (https://doi.org/10.32526/ennrj/20/202100228)

studies is that the higher the temperatures of the adsorption process are used, the lower the mechanical stability of chemical interaction between the support and the active site (Singh et al., 2019). Recently, ZnO on various base supports (e.g., activated carbon, zeolite, silicon dioxide, multiwall carbon nanotubes, and reduced graphite oxide) to remove H_2S at room temperature have been reported (de Falco et al., 2018; Geng et al., 2019; Singh et al., 2019). Hernández et al. (2011) used zinc oxide on activated carbon to remove H_2S (Hernández et al., 2011). Liu et al. (2012) implemented ZnO/SiO_2 gel composites to remove H_2S and the highest H_2S adsorption capacity was 96.4 mg/g (Liu et al., 2012). Song et al. (2013) removed hydrogen sulfide by zinc oxide/reduced graphite oxide composite (Song et al., 2013). Abdullah et al. (2018) reported the removal of hydrogen sulfide from biogas by using zinc oxide-impregnated zeolite with the maximum capacity of H_2S adsorption of 15.75 mg/g (Abdullah et al., 2018). Singh et al. (2019) used ZnO-decorated multiwall carbon nanotubes for efficient H_2S removal (Singh et al., 2019). Most recently, Geng and coworkers used a zinc oxide nanoparticle/ molecular sieve to remove hydrogen sulfide with the highest capacity of 54.9 mg/g (Geng et al., 2019).

Hydroxyapatite (HA) $Ca_{10}(PO_4)_6(OH)_2$ is the main component of bone and hard tissue of animals (Thien et al., 2015; Thien et al., 2021). HA nanoparticles are capable of binding to metal ions such as Zn^{2+}, Cd^{2+}, and Cu^{2+} (Ibrahim et al., 2020). HA nanomaterials have been synthesized by various methods including sol-gel, precipitation, hydrothermal, and microwave-assisted synthesis (Ibrahim et al., 2020; Thien et al., 2021). Significant advantages of the precipitation method for synthesizing HA are that it is simple, cost-effective, and highly repeatable. Moreover, this method can be used to extract HA from bio-wastes such as eggshell, cow bone, coral, shells, and especially fish scales, major wastes in aquatic product processing (Kongsri et al., 2013; Thien et al., 2021).

In this study, HA was extracted from the scales of red tilapia (*Oreochromis* sp.), the most popular freshwater fish in the Mekong Delta, Vietnam. Next, HA was combined with a precursor of zinc nitrate under appropriate conditions to prepare ZnO/HA materials available for the removal of H_2S. Finally, ZnO/HA materials were applied to remove H_2S at ambient conditions.

2. METHODOLOGY

2.1 Materials

Hydrochloric acid (HCl), sodium hydroxide (NaOH), ammonium hydroxide (NH_4OH) (28-30%), and zinc nitrate hexahydrate ($Zn(NO_3)_2 \cdot 6H_2O$) (99%) were purchased from Merck. Distilled water was used for all experiments. Hydrogen sulfide and nitrogen were supplied by a local company in Vietnam.

2.2 Methods

2.2.1 Preparation of hydroxyapatite nano-powders from fish scales

The scales of red tilapia (*Oreochromis* sp.) were collected from a local market in Ninh Kieu District, Can Tho City, Vietnam. They were soaked and rinsed in distilled water several times to remove salts and dirty substances. To deprotein, the scales were soaked and stirred in 0.1 M HCl solution for 15 min at room temperature and washed several times with distilled water. The residue of HCl was neutralized by 5% (w/v) NaOH solution. The remaining proteins of fish scales were treated with 50% (w/v) NaOH, heated and stirred at 100°C for 80 min. The precipitated (nanopowder) particles were filtered and washed with distilled water before being dried at 60°C (Kongsri et al., 2013; Zainol et al., 2019).

2.2.2 Preparation of ZnO/hydroxyapatite nano-powders

ZnO/hydroxyapatite nanopowders were prepared via a two-step in-situ deposition of $Zn(NO_3)_2$ on HA nanoparticles by a reaction with NH_4OH. Briefly, HA (1 g) was added to 50 mL of $Zn(NO_3)_2$ solution with the weight percent ZnO: HA ratios of 5/95, 15/85, and 30/70. Then, NH_4OH (25%) was added slowly to the solution until pH reached 10 under continuous stirring of 200 rpm for 24 h at room temperature. The precipitate was washed with distilled water several times. Finally, the precipitate was calcined at 500°C for 3 h.

2.2.3 Characterization of hydroxyapatite nano-powders and ZnO/hydroxyapatite nanopowders

Phase structures of HA and ZnO/HA materials were analyzed by X-ray diffraction (XRD, D8 Advance Brucker, Germany). XRD results were obtained for samples of HA and ZnO/HA at 2 theta in the range of 10°-70°.

The functional groups of HA and the interaction between ZnO and HA were characterized by Fourier transform infrared spectroscopy (FTIR, Nicolet 6700, Thermo Scientific).

Surface morphology of the hydroxyapatite and ZnO/HA nanopowders were observed by a scanning electron microscopy (SEM, JSM-6390LV, JEOL, Japan) at an accelerating voltage of 10 kV after gold coating.

2.2.4 Removal of H_2S

The adsorption experiments are described in Figure 1. The system consists of three main components: two gas cylinders for supplying a mixture of H_2S and nitrogen, a reactor (U-shaped Pyrex glass tube with an internal diameter of 8 mm and length of 30 cm), and a H_2S sensor (Alphasense company, England). To study H_2S adsorption ability, ZnO/HA samples (0.5 g) with ZnO/HA mass ratios of 5%, 10%, and 15% were fixed in the reactor. Experiments were carried out with an inlet H_2S concentration of 1,450 ppmv at ambient conditions (30°C, 1 atm). The sulfur adsorption capacity (SC) at the breakthrough point of the materials was determined by the following equation (Abdullah et al., 2018):

$$SC\left(\frac{g-sulfur}{100\ g-sorbent}\right) = WHSV \times \frac{M_S}{V_{mol}} \times \int_0^t (C_{in} - C_{out}) \times 10^{-4} dt \quad (1)$$

Where; WHSV is the weight hourly space velocity fixed at 0.176 (L/(min·g); M_S is the standard atomic weight of sulfur (32 g/mol); C_{in} is the inlet concentration of H_2S (1,450 ppmv); C_{out} is the outlet concentration of H_2S at the breakthrough point (ppmv); V_{mol} is the molar volume (24.5 L/mol) at standard condition (298 K and 1 atm); t is time of the adsorption until H_2S concentration in the output gases is higher than the breakthrough time (min).

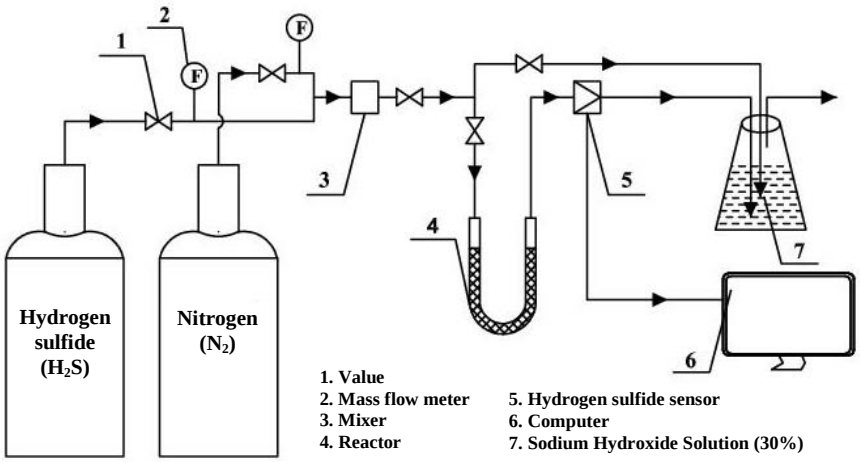

Figure 1. The experimental system for removing hydrogen sulfide

3. RESULTS AND DISCUSSION

3.1 Structural characterization of hydroxyapatite nanopowders and hydroxyapatite/ZnO nanopowders

Figure 2 shows XRD patterns of HA and HA/ZnO hydroxyapatite nanopowders with mass ratios of 5%, 15%, and 30%. From the XRD patterns, the intensities of the characteristic peaks of ZnO increased with the increase in concentrations of ZnO. The diffraction peaks at the 2θ of 25.9°, 31.78°, 32.15°, 32.83°, 34.04°, 39.70°, 46.68°, 49.39°, and 53.10° corresponding to the lattice planes of (002), (211), (112), (300), (202), (310), (222), (213), and (004), respectively could be exactly assigned to the HA phase (JCPDS No: 00-009-0432). The crystalline phase of ZnO can be observed at the 2θ of 31.7°, 34.4°, 36.3°, 47.5°, 56.6°, 62.9°, 66.4°, 67.9°, and 69.1° corresponding to the lattice planes of (100), (002), (101), (102), (110), (103), (200), (112), and (201) (JCPDS No: 36-1451). Thus, loaded ZnO based on HA materials were successfully prepared. To further understand the interactions between ZnO and HA as well as their morphologies, HA and ZnO/HA materials were characterized using FTIR and SEM methods.

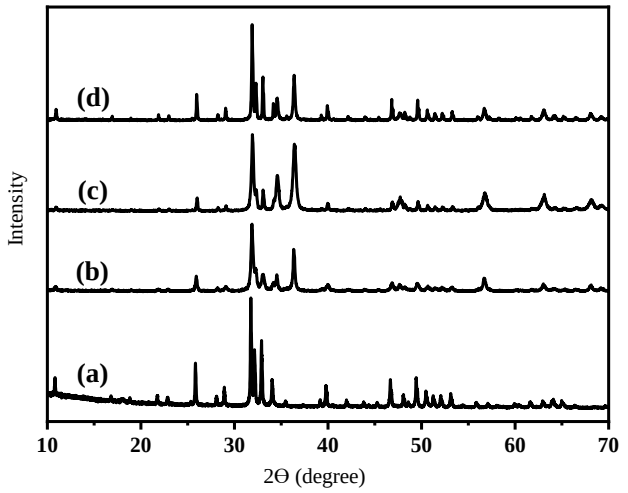

Figure 2. XRD patterns of HA and HA/ZnO nanopowders: (a) HA, (b) ZnO (5 wt%)/HA, (c) ZnO (15 wt%)/HA, and (d) ZnO (30 wt%)/HA

Figure 3 shows the FTIR spectra of HA and ZnO/HA particles. The functional groups OH^- and PO_4^{3-} of HA were characterized by oscillations at wavelengths 3,570 and 3,439 cm^{-1}. The characteristic P-O absorbances of PO_4^{3-} groups are at wavelengths 568, 603, 633, 1,035, 1,995 cm^{-1}. In the spectra, there are also typical fluctuations of CO_3^{2-} groups detected at the wavelength of 1,456 cm^{-1}, which indicates the presence of type B-HA, i.e., PO_4^{3-} functional groups are replaced by CO_3^{2-} functional groups. This result is completely consistent with that of Kongsri et al. (2013). In addition, no other strange vibrations were found in FTIR suggesting that HA material prepared from fish scales by the alkali heat method did not show the presence of other impurities. The FT-IR diagram of ZnO/HA in Figure 3(b) shows the functional groups are similar to those in Figure 3(a). This means that in the process of loading ZnO on HA, the functional groups of HA material were not changed (Saleh, 2011; Saleh, 2015a; Saleh, 2015b). However, from the FT-IR spectrum of ZnO/HA materials, the intensity of the oscillations of the PO_4^{3-} groups increases compared to that of HA material due to the connection between zinc and PO_4^{3-} groups (Zhou et al., 2008).

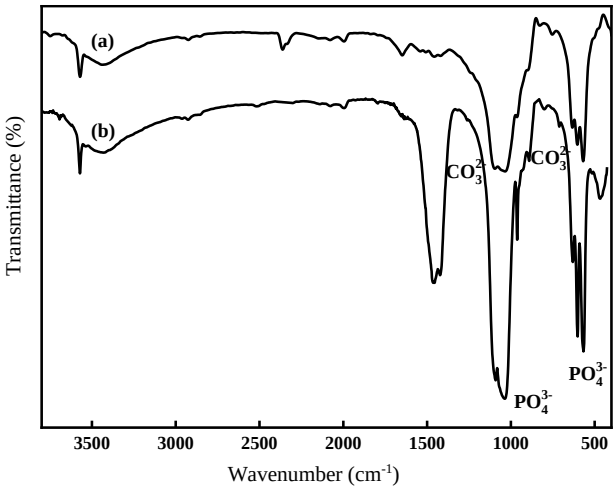

Figure 3. FTIR spectra: (a) HA and (b) ZnO (15 wt%)/HA

Figure 4 shows SEM images of synthesized HA and ZnO/HA. The morphology of HA and ZnO based on HA materials was the same. However, in Figure 4(b), the ZnO nanoparticles were uniformly deposited on the surface of the HA. The results were consistent with previous reports (Kongsri et al., 2013; Saleh, 2016; Saleh, 2018). Also, the specific surface area of HA was 37.022 m^2/g and ZnO/HA was 110.609 m^2/g. Thus, the H_2S adsorption capacity of ZnO/HA could be improved due to the enhanced surface area to volume ratio of the material.

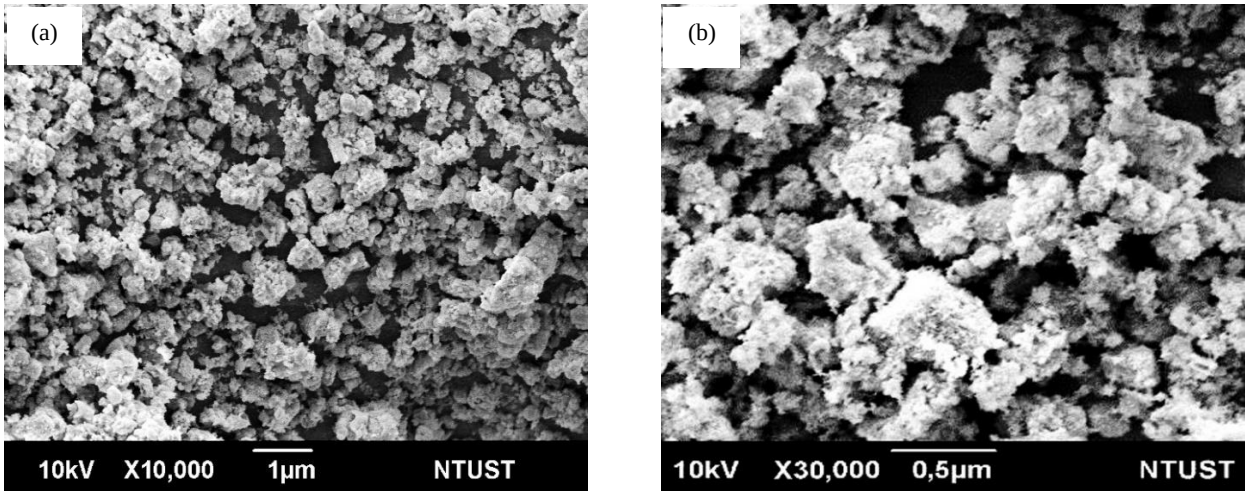

Figure 4. SEM images of (a) HA and (b) ZnO (15 wt%)/HA

3.2 Hydrogen sulfide adsorption capacity

The breakthrough curves of hydrogen sulfide for various samples of ZnO (5, 15, 30 wt%)/HA are shown in Figure 5(a). From the breakthrough curves of hydrogen sulfide, the corresponding adsorption capacities were determined according to Equation 1 and shown in Figure 5(b). At low loading ZnO, the adsorption capacity is low. When increasing ZnO content, the adsorption capacity increases and reaches a maximum value of 26.3 mg S/g sorbent for sample ZnO (15 wt%)/HA, then decreases with increasing ZnO content. Due to chemical affinity of ZnO to H_2S, the adsorption capacity increases when more ZnO is added. However, at the high content of ZnO loading, the excess of ZnO might agglomerate and collapse the active centers for desulphurization. Also, with 3 replicates in each sample, the difference is not significant. The results are in good agreement with previous studies (Abdullah et al., 2018; Geng et al., 2019; Liu et al., 2012; Saleh, 2021a; Saleh and Al-Hammadi, 2021; Wang et al., 2008). Therefore, 15 wt% of ZnO loaded on HA is the optimum content for the effective removal of H_2S.

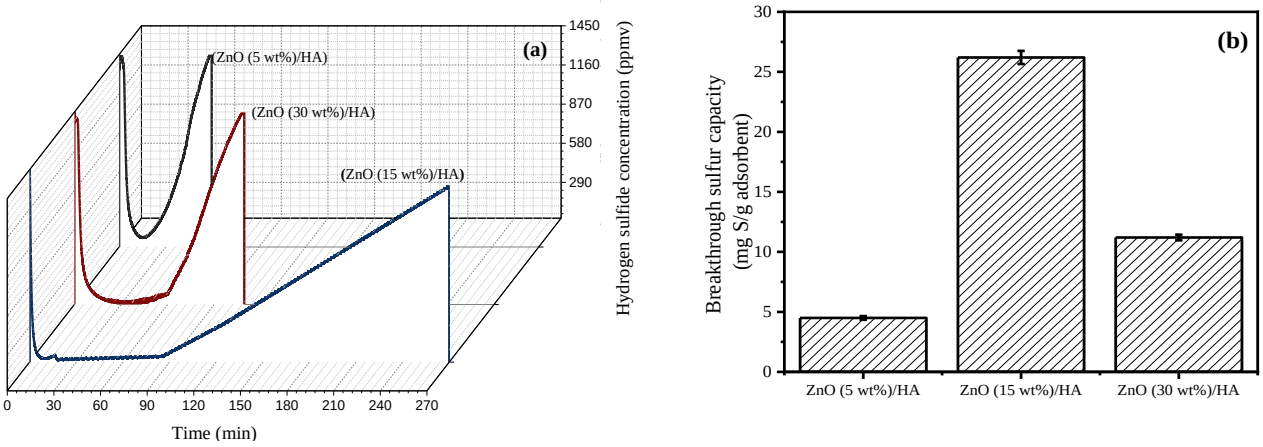

Figure 5. (a) The breakthrough curves of hydrogen sulfide with different ZnO loading (5, 15, 30 wt%) on HA nanoparticles; (b) The sulfur adsorption capacities of the different ZnO loading (5, 15, 30 wt%) on HA nanoparticles with 3 replicates (all experiments were carried out with an inlet H_2S concentration of 1,450 ppmv at 30°C, 1 atm)

Table 1 shows the adsorption capacity and the breakthrough time of (ZnO 15 wt%)/HA nanoparticles at the breakthrough point as well as ZnO based on some other carriers such as MCM-41, BSA-15, SiO_2, activated carbon, zeolite Na-A, and Zn-MOF reported in several studies for comparison. The adsorption capacity of ZnO based on HA is higher than that of ZnO based on MCM-41, BSA-15, activated carbon, and zeolite Na-A and lower than that of ZnO based on SiO_2 or activated carbon. It may be explained by the interactions between ZnO and carriers and by different morphologies and sizes of the sorbents. Thus, ZnO (15 wt%)/HA nanoparticles would be a promising material for the removal of H_2S.

Table 1. Sulfur capacities of sorbents based on ZnO at room temperature

Adsorbent	Sulfur adsorption capacity (mg S/g adsorbent)	Temperature (°C)	Breakthrough time (min)	References
ZnO (15 wt%)/MCM-41	5.9	25	~70	Hussain et al. (2012)
ZnO (15 wt%)/SBA-15-S	18.5	25	~200	Hussain et al. (2012)
ZnO (15 wt%)/SBA-15-F	15.6	25	~180	Hussain et al. (2012)
ZnO (15 wt%)/SiO_2	32.0	-	19	Dhage et al. (2010)
ZnO (20 wt%)/Activated carbons	17.1	30	2	de Falco et al. (2018)
ZnO (20 wt%)/Zeolite Na-A	24.0	28	60	Abdullah et al. (2018)
ZnO/Activated carbons	66.4	30	150	Yang et al. (2019)
ZnO-MgO (20 wt%)/Activated carbon	96.5	30	124	Yang et al. (2020)
Zn-MOF/ZnO nanocomposites	14.2	Ambient conditions	~11	Gupta et al. (2021)
ZnO (15 wt%)/HA	26.3	30	85	This work

4. CONCLUSION

High purity HA nanoparticles were successfully extracted from red tilapia scales, an abundant organic waste in the Mekong delta. From the obtained HA nanoparticles, ZnO/HA nanoparticles were also successfully prepared with a uniform ZnO loading of 5, 15, and 30 wt%. The uniform distribution of ZnO on HA, confirmed by SEM image analysis, facilitated the H_2S adsorption in a gas mixture. The adsorption processes at ambient conditions (30°C, 1 atm) were very useful in practical applications. Based on the adsorption capacity experiment results with different ZnO loadings, the 15 wt% ZnO/HA sample was found optimal with the maximum adsorption capacity for H_2S at the breakthrough point of 26.5 mg S/g adsorbent. This breakthrough sulfur capacity was the highest capacity ever reported for ZnO using HA as an effective carrier. Thus, ZnO/HA nanoparticles showed great potential in H_2S removal and the sustainable use of the enormous source of red tilapia scales.

ACKNOWLEDGEMENTS

This work was financially supported by the "Can Tho University Improvement Project VN14-P6, supported by a Japanese ODA loan", under grant number E7.

CONFLICT OF INTEREST

The authors declare that there is no conflict of interest.

REFERENCES

Abdullah AH, Mat R, Somderam S, Abd Aziz AS, Mohamed A. Hydrogen sulfide adsorption by zinc oxide-impregnated zeolite (synthesized from Malaysian kaolin) for biogas desulfurization. Journal of Industrial and Engineering Chemistry 2018;65:334-42.

Ali I, Al-Arfaj AA, Saleh TA. Carbon nanofiber-doped zeolite as support for molybdenum based catalysts for enhanced hydrodesulfurization of dibenzothiophene. Journal of Molecular Liquids 2020a;304:Article No. 112376.

Ali I, Al-Shafei EN, Al-Arfaj AA, Saleh TA. Influence of titanium oxide on the performance of molybdenum catalysts loaded on zeolite toward hydrodesulfurization reactions. Microporous and Mesoporous Materials 2020b;303:Article No. 110188.

Ali I, Saleh TA. Zeolite-graphene composite as support for molybdenum-based catalysts and their hydrodesulfurization performance. Applied Catalysis A: General 2020;598:Article No. 117542.

Al-Hammadi SA, Al-Amer AM, Saleh TA. Alumina-carbon nanofiber composite as a support for MoCo catalysts in hydrodesulfurization reactions. Chemical Engineering Journal 2018;345:242-51.

Al-Jamimi HA, Saleh TA. Transparent predictive modelling of catalytic hydrodesulfurization using an interval type-2 fuzzy logic. Journal of Cleaner Production 2019;231:1079-88.

Buazar F, Alipouryan S, Kroushawi F, Hossieni SA. Photo-degradation of odorous 2-mercaptobenzoxazole through zinc oxide/hydroxyapatite nanocomposite. Applied Nanoscience 2015;5(6):719-29.

Buazar F, Baghlani-Nejazd MH, Badri M, Kashisaz M, Khaledi-Nasab A, Kroushawi F. Facile one-pot phytosynthesis of magnetic nanoparticles using potato extract and their catalytic activity. Starch-Stärke 2016a;68(7-8):796-804.

Buazar F, Bavi M, Kroushawi F, Halvani M, Khaledi-Nasab A, Hossieni SA. Potato extract as reducing agent and stabiliser in a facile green one-step synthesis of ZnO nanoparticles. Journal of Experimental Nanoscience 2016b;11(3):175-84.

de Falco G, Montagnaro F, Balsamo M, Erto A, Deorsola FA, Lisi L, et al. Synergic effect of Zn and Cu oxides dispersed on activated carbon during reactive adsorption of H_2S at room temperature. Microporous and Mesoporous Materials 2018; 257:135-46.

Dhage P, Samokhvalov A, Repala D, Duin EC, Bowman M, Tatarchuk BJ. Copper-promoted ZnO/SiO_2 regenerable sorbents for the room temperature removal of H_2S from reformate gas streams. Industrial and Engineering Chemistry Research 2010;49(18):8388-96.

Geng Q, Wang LJ, Yang C, Zhang HY, Zhao YR, Fan HL, et al. Room-temperature hydrogen sulfide removal with zinc oxide nanoparticle/molecular sieve prepared by melt infiltration. Fuel Processing Technology 2019;185:26-37.

Gupta NK, Bae J, Kim S, Kim KS. Fabrication of Zn-MOF/ZnO nanocomposites for room temperature H_2S removal: Adsorption, regeneration, and mechanism. Chemosphere 2021;274:Article No. 129789.

Han X, Chen H, Liu Y, Pan J. Study on removal of gaseous hydrogen sulfide based on macroalgae biochars. Journal of Natural Gas Science and Engineering 2020;73:Article No. 103068.

Hernández SP, Chiappero M, Russo N, Fino D. A novel ZnO-based adsorbent for biogas purification in H_2 production systems. Chemical Engineering Journal 2011;176-177:272-9.

Hussain M, Abbas N, Fino D, Russo N. Novel mesoporous silica supported ZnO adsorbents for the desulphurization of biogas at low temperatures. Chemical Engineering Journal 2012;188:222-32.

Ibrahim M, Labaki M, Giraudon JM, Lamonier JF. Hydroxyapatite, a multifunctional material for air, water and soil pollution control: A review. Journal of Hazardous Materials 2020;383:Article No. 121139.

Kongsri S, Janpradit K, Buapa K, Techawongstien S, Chanthai S. Nanocrystalline hydroxyapatite from fish scale waste: Preparation, characterization and application for selenium adsorption in aqueous solution. Chemical Engineering Journal 2013;215:522-32.

Liu G, Huang Z-H, Kang F. Preparation of ZnO/SiO_2 gel composites and their performance of H_2S removal at room temperature. Journal of Hazardous Materials 2012;215-216:166-72.

Qiu B, Tao X, Wang H, Li W, Ding X, Chu H. Biochar as a low-cost adsorbent for aqueous heavy metal removal: A review. Journal of Analytical and Applied Pyrolysis 2021;155:Article No. 105081.

Quan W, Jiang X, Wang X, Song C. Hydrogen sulfide removal from biogas on ZIF-derived nitrogen-doped carbons. Catalysis Today 2021;371:221-30.

Saleh TA. Carbon nanotube-incorporated alumina as a support for MoNi catalysts for the efficient hydrodesulfurization of thiophenes. Chemical Engineering Journal 2021a;404:Article No. 126987.

Saleh TA. Isotherm, kinetic, and thermodynamic studies on Hg(II) adsorption from aqueous solution by silica-multiwall carbon nanotubes. Environmental Science and Pollution Research 2015a;22(21):16721-31.

Saleh TA. Nanocomposite of carbon nanotubes/silica nanoparticles and their use for adsorption of Pb(II): From surface properties to sorption mechanism. Desalination and Water Treatment 2016;57(23):10730-44.

Saleh TA. Nanomaterials: Classification, properties, and environmental toxicities. Environmental Technology and Innovation 2020;20:Article No. 101067.

Saleh TA. Protocols for synthesis of nanomaterials, polymers, and green materials as adsorbents for water treatment technologies. Environmental Technology and Innovation 2021b;24:Article No. 101821.

Saleh TA. Mercury sorption by silica/carbon nanotubes and silica/activated carbon: A comparison study. Journal of Water Supply: Research and Technology-Aqua 2015b;64(8):892-903.

Saleh TA. Simultaneous adsorptive desulfurization of diesel fuel over bimetallic nanoparticles loaded on activated carbon. Journal of Cleaner Production 2018;172:2123-32.

Saleh T. The influence of treatment temperature on the acidity of MWCNT oxidized by HNO_3 or a mixture of HNO_3/H_2SO_4. Applied Surface Science 2011;257:7746-51.

Saleh TA, Al-Hammadi SA. A novel catalyst of nickel-loaded graphene decorated on molybdenum-alumina for the HDS of liquid fuels. Chemical Engineering Journal 2021;406:Article No. 125167.

Saleh TA, Al-Hammadi SA, Al-Amer AM. Effect of boron on the efficiency of MoCo catalysts supported on alumina for the hydrodesulfurization of liquid fuels. Process Safety and Environmental Protection 2019;121:165-74.

Saleh TA, Sulaiman KO, Al-Hammadi SA. Effect of carbon on the hydrodesulfurization activity of MoCo catalysts supported on zeolite/active carbon hybrid supports. Applied Catalysis B: Environmental 2020;263:Article No. 117661.

Singh A, Pandey V, Bagai R, Kumar M, Christopher J, Kapur GS. ZnO-decorated MWCNTs as solvent free nano-scrubber for efficient H_2S removal. Materials Letters 2019;234:172-4.

Song HS, Park MG, Kwon SJ, Yi KB, Croiset E, Chen Z, et al. Hydrogen sulfide adsorption on nano-sized zinc oxide/reduced graphite oxide composite at ambient condition. Applied Surface Science 2013;276:646-52.

Thien DVH, Ho MH, Hsiao SW, Li CH. Wet chemical process to enhance osteoconductivity of electrospun chitosan nanofibers. Journal of Materials Science 2015;50(4):1575-85.

Thien DVH, Thuyen NTB, Quyen TTB, Chiem NH, Thuy VPD, Viet PH. Microwave-assisted synthesis of nanorod hydroxyapatite from eggshells. Vietnam Journal of Science, Technology and Engineering 2021;63(1):3-6.

Wang X, Sun T, Yang J, Zhao L, Jia J. Low-temperature H_2S removal from gas streams with SBA-15 supported ZnO nanoparticles. Chemical Engineering Journal 2008;142(1): 48-55.

Wang Y-C, Han M-F, Jia T-P, Hu X-R, Zhu H-Q, Tong Z, et al. Emissions, measurement, and control of odor in livestock farms: A review. Science of the Total Environment 2021; 776:Article No. 145735.

Yang C, Yang S, Fan H, Wang Y, Shangguan J. Tuning the ZnO-activated carbon interaction through nitrogen modification for enhancing the H_2S removal capacity. Journal of Colloid and Interface Science 2019;555:548-57.

Yang C, Wang Y, Fan H, de Falco G, Yang S, Shangguan J, et al. Bifunctional ZnO-MgO/activated carbon adsorbents boost H_2S room temperature adsorption and catalytic oxidation. Applied Catalysis B: Environmental 2020;266:Article No.118674.

Zainol I, Adenan NH, Rahim NA, Jaafar CNA. Extraction of natural hydroxyapatite from tilapia fish scales using alkaline treatment. Materials Today: Proceedings 2019;16:1942-8.

Zhou G, Li Y, Xiao W, Zhang L, Zuo Y, Xue J, et al. Synthesis, characterization, and antibacterial activities of a novel nano-hydroxyapatite/zinc oxide complex. Journal of Biomedical Materials Research Part A 2008;85(4):929-37.